UNIVERSITY OF CALIFORNIA SAN DIEGO

Biochemical Analysis of Cockayne Syndrome-related CSB Mutants and CSB Regulation in Yeast

A Thesis submitted in partial satisfaction of the requirements

for the degree of Master of Science

in

Biology

by

Bernice Leung

Committee in Charge:

Professor Dong Wang, Chair
Professor James Kadonaga, Co-Chair
Professor Nan Hao

2020

The Thesis of Bernice Leung is approved, and it is acceptable in quality and form for publication on microfilm and electronically:

_____

_____

Co-Chair

_____

Chair

University of California San Diego

2020

TABLE OF CONTENTS

LIST OF FIGURES

LIST OF TABLES

ACKNOWLEDGEMENTS

I would like to acknowledge Professor Dong Wang for his support as the chair of my committee. I would also like to express my gratitude to Dr. Jun Xu and Dr. Juntaek Oh for their research mentorship and guidance in writing this thesis. This work was supported by National Institutes of Health Grant R01 GM102362 (to D.W.).

Chapter 2 is co-authored with Xu, Jun. The thesis author was the primary author of this chapter.

ABSTRACT OF THE THESIS

Biochemical Analysis of Cockayne Syndrome-related
CSB Mutants and CSB Regulation in Yeast

by

Bernice Leung

Master of Science in Biology

University of California San Diego, 2020

Professor Dong Wang, Chair
Professor James Kadonaga, Co-Chair

During transcriptional elongation, RNA Polymerase (Pol II) may become stalled at DNA lesions. One way to resolve this transcriptional arrest is through Transcription Coupled-Nucleotide Excision Repair (TC-NER). Cockayne Syndrome Group B protein (CSB) is the

first protein to be recruited and binds the upstream of stalled Pol II, alters the surrounding chromatin environment and allows other repair factors to access the DNA lesion. Many mutations in CSB are associated with Cockayne Syndrome (CS). Chapter 1 investigates the biochemical properties of CSB mutations observed in CS patients using Rhp26, the *Schizosaccharomyces pombe* ortholog of CSB. All six mutations studied show a decrease in chromatin remodelling and DNA translocation activities, both of which are important activities for CSB to execute its molecular function. In Chapter 2, we studied the regulation of CSB/Pol II interactions by its flanking regions using Rad26, the *Saccharomyces cerevisiae* ortholog of CSB. A conserved C-terminal region coupling motif promotes Rad26/Pol II interactions. Taken together, these results demonstrate that mutations to CSB that can be detrimental to its enzymatic activity and its role in maintaining genomic fidelity.

INTRODUCTION

Maintenance of genomic fidelity is important for the correct transmission and interpretation of genetic information from parent to progeny. DNA damage can be caused by UV exposure, endogenous metabolic byproducts of the cell, or from exposure to exogenous sources such as chemotherapeutic agents (Hanawalt and Spivak, 2008). Cells have a variety of methods to repair damage and mistakes made in the flow of genetic information. These repair mechanisms can be categorized by their substrates. Bulkier, helix distorting damages such as pyrimidine dimers are repaired through Nucleotide Excision Repair (NER) (Licht et al., 2003). Free radicals or alkylating agents that cause small, non-helix distorting damages such as abasic sites or single-stranded breaks are repaired through Base Excision Repair (Chatterjee and Walker, 2017). Double-stranded breaks can be repaired through either homologous recombination, or non-homologous end joining (Chatterjee and Walker, 2017).

NER can be further divided into two sub-pathways: global genome NER (GG-NER) and transcription-coupled NER (TC-NER) (Kusakabe et al., 2019). While these two sub-pathways share the same spectrum of substrates and downstream steps for lesion excision and repair (Marteijn et al., 2014), they have distinct damage recognition steps. Damage recognition is independent of transcription in GG-NER, whereas a stalled RNA Polymerase II (Pol II) at a DNA damage site serves as a recognition signal in TC-NER. TC-NER also preferentially repair DNA lesions located on the transcribing strand (Leadon and Lawrence, 1992).

Cockayne Syndrome Group B protein (CSB) is the first protein recruited to a stalled Pol II (Hanawalt and Spivak, 2008). CSB, also known as *ERCC6*, is highly conserved from yeast to humans. CSB belongs to the SNF2-like family under the Superfamily 2 (SF2) helicases (Gorbalenya and Koonin, 1993). Some other commonly known SF2 family members include SWI/SNF, ISWI, and HARP (Eisen et al., 1995). SNF2-like family

members are characterized by a core domain that consists of two Rec-A like domains, termed lobes 1 and 2 (Hauk and Bowman, 2011). Seven distinct helicase motifs (motif I, Ia, II, III, IV, V, and VI) are also conserved across SNF2-like family members, with motifs I, Ia, II and III located in lobe 1 and motifs IV, V and VI located in lobe 2 (Thoma et al., 2005). In order for repair machinery to access DNA lesions, CSB binds to the upstream of a stalled Pol II on the transcribing strand, alters the local chromatin structure and allows for the recruitment and access of other repair proteins to the damaged site (Newman et al., 2006). Most recently, it is found that that CSB recruits CSA through a novel CSA-interaction motif, which then recruits UVSSA and TFIIH to unwind DNA around the damaged site for repair access in humans (van der Weegen et al., 2020).

Malfunctioning of DNA repair mechanisms is the cause of a variety of DNA repair defect disorders, one of which is Cockayne Syndrome (CS). In humans, mutations in CSB are commonly associated with CS, a neurological disorder with symptoms such as photosensitivity and premature ageing (Karikkineth et al., 2017; Weidenheim et al., 2009). CS is categorized into three subtypes by age of onset and disease severity: CS type I, type II, also known as cerebro-oculo-facio-skeletal syndrome (COFS), and type III. Type II is the most severe subtype, with disease onset from birth; type I has delayed onset in the first two years of life, and type III presents as a milder version of CS type I (Nance and Berry, 1992). Because no cures exist for CS, the prognosis for CS patients remains poor; on average, CS patients live up to 12 years of age with good symptom management (Nance and Berry, 1992). The clinical phenotypes of CS patients are often a result of mutated CSB being unable to initiate TC-NER to repair DNA damage (Cleaver et al., 2009). Some CSB variants are associated with an increased risk for lung cancer, and CSB-knockout mice demonstrate increased sensitivity to oxidizing agents and susceptibility to skin cancer (de Waard et al., 2004; Ma et al., 2009). Some CS symptoms are also indicative of mitochondrial dysregulation, possibly due to the role of CSB in repairing oxidative DNA damage (Scheibye-

Knudsen et al., 2013; Wilson et al., 2016b). However, a complete absence of CSB in humans does not cause CS, suggesting that CS may not be entirely caused by defects in TC-NER, and that there might be redundancy in other pathways involving CSB (Horibata et al., 2004). It has also been suggested that CS could be an inflammatory disease, as CSB is found to upregulate the expression of genes involved in inflammatory pathways, and CSB-null cells are under inflammatory stress (Horibata et al., 2004). The same study also did not find any clear correlation between CSB and the expression of DNA repair genes, suggesting that the pathology of CS is more complex than we think (Horibata et al., 2004).

To elucidate the important role of CSB in TC-NER and the consequences of *ERCC6* gene mutations, we set out to examine the biochemistry and regulation of CSB through its two yeast orthologs, Rhp26 in fission yeast *Schizosaccharomyces pombe* and Rad26 in budding yeast *Saccharomyces cerevisiae*. The first chapter investigates the biochemistry of CS mutations identified in CSB using Rhp26. Understanding how these Rhp26 CS mutants function biochemically can lead to a better understanding of roles of CSB in transcription-coupled DNA repair and the pathology of Cockayne Syndrome. The second chapter explores the regulation of Rad26-Pol II interactions by its flanking regions. Understanding how these interactions are regulated can lead to a better understanding of the mechanism of Rad26 (CSB) recruitment to Pol II in TC-NER.

Chapter 1: Preliminary Biochemical Analysis of Cockayne Syndrome Related Rhp26 Mutations

1.1 Introduction

Cockayne Syndrome (CS) is an autosomal recessive neurodegenerative disorder, and CS patients are characterized by hallmark symptoms such as sunlight photosensitivity, premature aging, and impaired nervous system development (Karikkineth et al., 2017). Around 70% of CS cases are associated with mutations in the Cockayne Syndrome group B protein (CSB), a protein that serves as an initiating signal for transcriptional arrests to be resolved through transcription-coupled nucleotide excision repair (TC-NER) (Laugel, 2013). CSB is first recruited to the upstream of an arrested Pol II during transcription, and alters the surrounding chromatin environment to allow for the recruitment of other proteins and repair factors (Newman et al., 2006), (van der Weegen et al., 2020).

Specific CSB mutations have been identified in CS patients, but how these mutations affect the biochemical activities of CSB remains unknown (Cleaver et al., 2009). The difficulty of expression and purification of high quality and quantity of human CSB proteins represents a main hurdle for the full biochemical characterization of these mutations. To circumvent this problem, we took advantage of the fact that these mutations are often highly conserved across different species and generated them in Rhp26, the *Schizosaccharomyces pombe* ortholog of human CSB (Figure 1.1). Indeed, previous studies revealed a conserved leucine latch motif at the N terminus of Rhp26 has an important regulatory component of CSB (Wang et al., 2014). The leucine latch is shown to auto-inhibit ATPase and chromatin remodeling activities of Rhp26, and mutations to the leucine latch restored chromatin remodeling activity in Rhp26 (Wang et al., 2014).

Based on the proposed role of CSB in TC-NER, we hypothesize that Rhp26 CS mutants would show decreased DNA binding, chromatin remodelling and DNA translocase abilities. We indeed found that N475D and L774P have decreased DNA binding affinities, and all Rhp26 CS mutants tested have decreased chromatin remodelling and DNA translocase activities.

1.2 Materials and Methods

Identification, generation, and expression of Rhp26 Mutants

Missense mutations in Cockayne Syndrome Group B (CSB) proteins were identified from clinical reports (Table 1.1) (Laugel et al., 2010; Calmels et al., 2018; He et al., 2017; Wilson et al., 2016a). CSB and Rhp26 sequences were aligned to identify corresponding mutations in Rhp26 (Figure 1.1). Rhp26 mutants were generated by PCR with primers in Table 2.1 using the constitutively active $Rhp26^{\Delta 1\text{-}16}$ as the template. The constitutively active $Rhp26^{\Delta 1\text{-}16}$ was used as a positive control as it is does not contain the autoinhibitory leucine latch motif and has robust ATPase and chromatin remodeling activities (Wang et al., 2014). $Rhp26^{\Delta 1\text{-}16}$ was cloned into pGEX-6P1 followed by a PreScission Protease recognition sequence and an N-terminus His-GST tag. PCR generated Rhp26 mutants were confirmed with sequencing. Recombinant Rhp26 proteins were transformed into Rosetta 2 DE3 competent cells (Novagen) for expression. Cells were grown in LB at 37°C until OD_{600} reached 0.8 and protein expression was induced by 0.5 mM of IPTG at 25°C for 16 hours. Cells were lysed using a microfluidizer in lysis buffer (500 mM NaCl, 20 mM Tris-HCl (pH 7.5), 5% glycerol, 1 mM DTT). Lysate supernatant was applied to a Glutathione Sepharose column (GE Healthcare) and incubated at 4°C for 1 hour. The column was washed with 30 column volumes of purification buffer, followed by protein elution in elution buffer (lysis buffer

with 10 mM Glutathione (pH 7.5)) and overnight PreScission Protease digestion to remove N-terminal His-GST tag. Protein eluates were then equilibrated to 300 mM NaCl and loaded onto a HiTrap Heparin affinity column (GE Healthcare). Rhp26 mutants and Rhp26$^{\Delta 1\text{-}16}$ were eluted in a 300 - 1000 mM linear NaCl lysis buffer gradient. Protein purity was confirmed with SDS-PAGE.

Table 1.1. Rhp26 CS mutations studied.

Mutation	*S. pombe* #	Human #	Clinical Phenotype	Source
N to D	475	680	CS Type I with p.Arg68ProfsX13	Laugel et al (2010)
A to P	713	926	CS Type II with p.Phe665_Gln723del	Calmels et al (2018)
P to T	721	934	CS Type II in homozygous P934T	Wilson et al (2016)
V to G	744	957	CS Type I in homozygous V957G	Laugel et al (2010)
R to W	762	975	CS Type I with p.Arg612Ter	He et al (2017)
L to P	774	987	CS Type II with p.Met752_Gln762del	Laugel et al (2010)

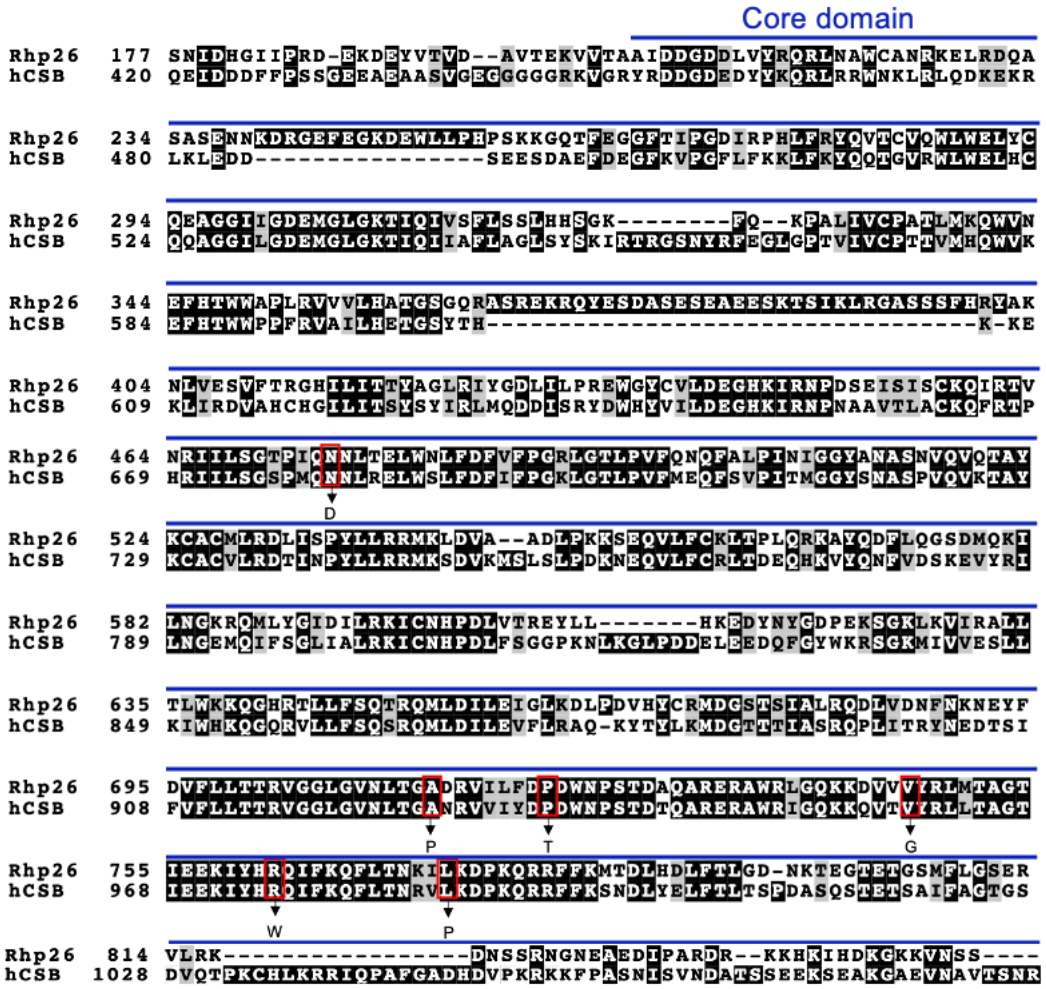

Figure 1.1. Sequence alignment of CSB with Rhp26. The highly conserved core domain in Rhp26, residues 205-851, is indicated in blue. The studied mutations are boxed in red, and the residue they are mutated to is indicated below each mutation.

Table 1.2. Primer sequences used in generating Rhp26 CS mutants.

	Forward Primer (5' to 3')	Reverse Primer (5' to 3')
N475D	GATCCAGGACAACCTTACCGAGCT TTGGAATTTATTTG	CGGTAAGGTTGTCCTGGATCGGAGT CCCTGAGAGGATA
A713P	TTGACTGGTCCTGACAGGGTAATT CTTTTTGATCC	TACCCTGTCAGGACCAGTCAAATTG ACTCCTAATC
P721T	CTTTTTGATACTGATTGGAATCCCT CAACGGATGC	TCCAATCAGTATCAAAAAGAATTACC CTGTCAGCAC
V744G	CTGGGCCAAAAGAAAGATGGAGTA GTTTATCGGTTGATG	CCATCTTTCTTTTGGCCCAGTCTCCA AGCACGTTC
R762W	ATTTATCATTGGCAAATCTTTAAGC AGTTTCTGACT	TAAAGATTTGCCAATGATAAATTTTT TCTTCAATA
L774P	TTGTTTTTTCCGCAAAGTTAGTAAT GCTCTAATAAC	TTGGATCTTTCGGAATTTTGTTAGTC AGAAACTGCTTA

Electrophoretic Mobility Shift Assay (EMSA)

Transcriptional scaffold was formed by annealing radioactively labelled RNA with template and non-template DNA at 95°C for 5 minutes, then slowly cooling down to room temperature. Rhp26$^{\Delta 1\text{-}16}$ and CS mutants of varying concentrations were incubated at room temperature with 10 nM radiolabelled scaffold for 30 minutes in EMSA buffer (20 mM Tris-HCl (pH 7.5), 50 mM NaCl, 5% glycerol, 0.5 mg/ml BSA) resolved on a 5% native PAGE in 0.5X TBE buffer (pH 8.0) and visualized using a phosphor screen and PharosFX imager.

Restriction Enzyme Accessibility Assay (REAA)

Salt-dialysis reconstituted chromatin was incubated with 100 nM Rhp26$^{\Delta 1\text{-}16}$ and CS mutants at room temperature in reaction buffer (1X NEB CutSmart Buffer, 3 mM ATP, 2 mM DTT, 5% glycerol, 15U HaeIII, 50 nM reconstituted nucleosomes). Reactions were carried out for an hour and quenched with stop buffer (20 mM Tris-HCl (pH 7.5), 1% SDS, 0.1 mg/ml glycogen, 0.8 U Proteinase K). DNA was extracted using phenol-chloroform extraction and ethanol precipitation, resolved on a 1% TBE agarose gel and visualized with GelRed staining. Statistical significance was calculated using a two-tailed T-test.

Triplex Disruption Assay

Triple helix was annealed by incubating a double stranded DNA tract (ds150) and radiolabelled Triplex Forming Oligo (TFO) in a 2:1 molar ratio in annealing buffer (33 mM Tris-Acetate (pH 5.5), 66 mM potassium acetate, 100 mM NaCl, 10 mM $MgCl_2$, 0.4 mM spermine) at a 59°C water bath allowed to slowly cool to room temperature overnight (Figure 2.2). 10 nM of radiolabelled triplex is incubated with 100 nM of Rhp26$^{\Delta 1\text{-}16}$ and CS mutants at room temperature in reaction buffer (36 mM Tris-Acetate (pH 6.9), 10 mM potassium acetate, 8 mM $MgCl_2$, 5% glycerol, 0.1 mg/ml BSA) for 30 minutes and quenched with stop buffer (reaction buffer with 1% SDS and 4 U Proteinase K). Reactions were resolved on an 8% PAGE with 40 mM Tris-Acetate (pH 6.9) and 1 mM $MgCl_2$ at 4°C for 2 hours and visualized using a phosphor screen and PharosFX imager. Results were quantified using Bio-Rad ImageLab. Statistical significance was calculated using a two-tailed T-test.

Figure 1.2. Schematic of triple helix for TFO displacement. The double stranded DNA tract (ds150) is labelled in red, and the TFO is labelled in blue.

1.3 Results

1.3.1 Localization of Rhp26/CSB Mutations

Details of the six missense mutations studied are outlined in Table 1.2 and Figure 1.2. Two mutations are homozygous CSB mutations, while the other four are coupled with frame shift, deletion and nonsense mutation to produce respective clinical phenotypes. There is no apparent correlation between zygosity and disease severity, as all subtypes of CS are found in both homozygous and compound heterozygous patients (Laugel et al., 2010). All six mutations studied are located within the core ATPase region of Rhp26 (Figure 1.3D) and are highly conserved among mammalian CSB proteins (Figure 1.1). In fact, a majority of CSB missense mutations involved in CS cases are located within the CSB core (Nance and Berry, 1992; Lake and Fan, 2013; Laugel et al., 2010). Two of the mutations, Asn680 and Ala926 (Asn475 and Ala713 in *S. pombe*) are located in the helicase motifs III and V respectively.

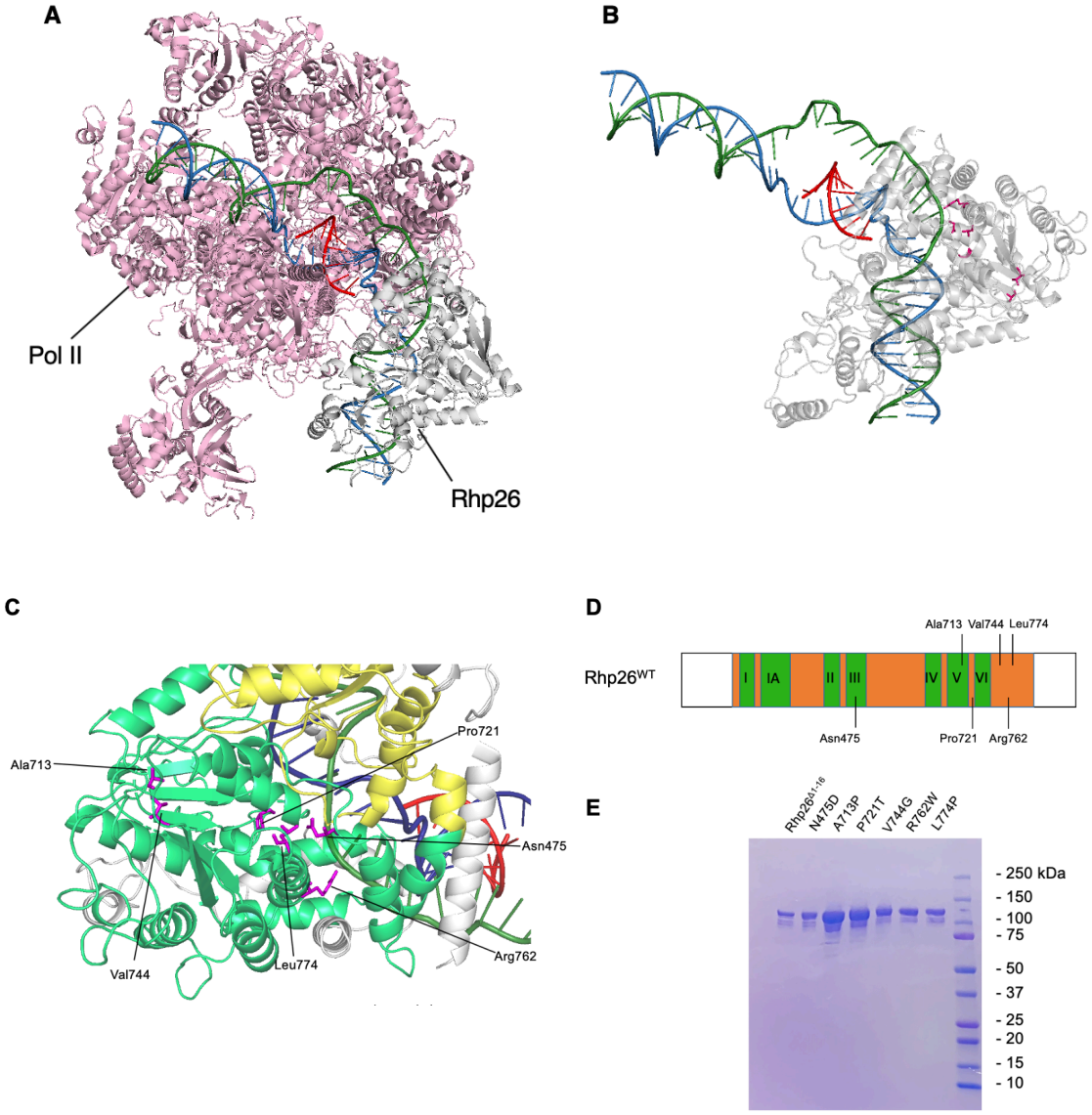

Figure 1.3. Localization of Rhp26 mutations in this study. (A) Rhp26 (grey) complexed with RNA Polymerase II (light pink) and a transcriptional scaffold (PDB ID: 5VVR) (Xu et al., 2017). The structure of Rhp26 is generated by homology modelling with 5VVR as template (Waterhouse et al., 2018). The template strand, non-template strand and RNA are colored in blue, dark green and red respectively. (B) Overall structure of Rhp26 with the six mutations studied shown in magenta. (C) Close up of the studied disease mutations in Rhp26. Lobes 1 and 2 of the Rhp26 core domain are colored in yellow and green respectively. (D) Domain architecture of Rhp26^{WT}. The ATPase domain is shown in orange and conserved helicase motifs among the SNF2-like family are labelled and shown in green. (E) SDS-PAGE of purified Rhp26$^{\Delta 1\text{-}16}$ and Rhp26 CS mutants. Rhp26 suffers from a small degree of C-terminal degradation *in vitro*.

1.3.2 Biochemical Analysis of Rhp26/CSB Mutations

We first compared the effect of Rhp26 point mutations on the DNA binding affinity of Rhp26. As shown in Figure 1.4, we observed reductions in DNA binding affinity in Rhp26 CS mutants N475D and L774P compared to Rhp26$^{\Delta 1\text{-}16}$. We observed almost no free DNA band left in the presence of 200 nM or 400 nM Rhp26$^{\Delta 1\text{-}16}$, suggesting that there is formation of Rhp26-DNA complexes. In contrast, we found almost no Rhp26-DNA complexes bands for the two Rhp26 mutants N475D and L774P under the same conditions. Note that we observed smear bands for the positive control Rhp26$^{\Delta 1\text{-}16}$, despite multiple repeats and extensive condition optimizations. These smear bands suggest the Rhp26-DNA complexes are likely partially dissociated during EMSA assay conditions.

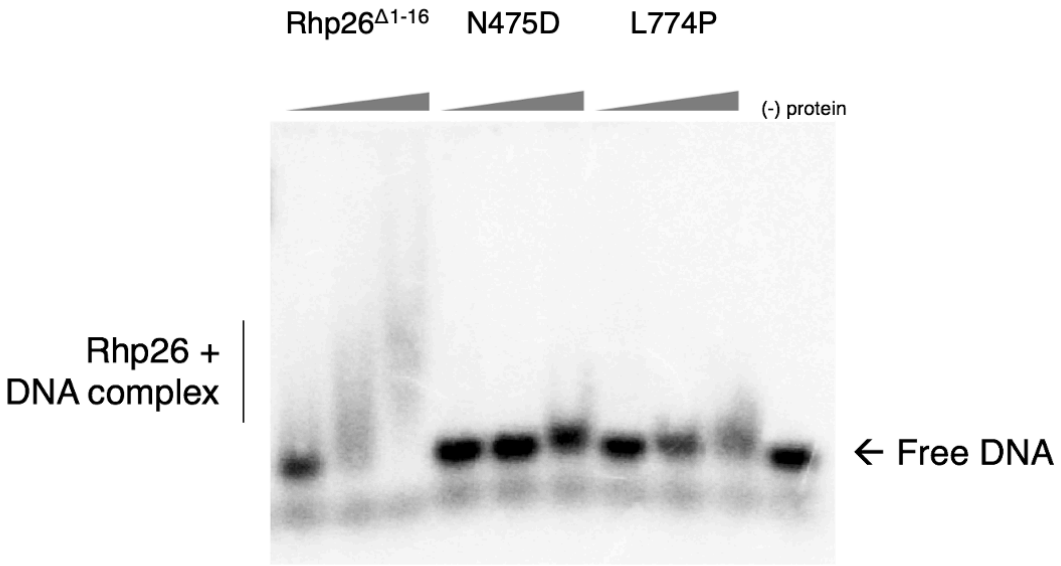

Figure 1.4. DNA binding affinity in Rhp26 CS mutants N475D and L774P assessed by EMSA. Protein concentrations of 100, 200 and 400 nM were used.

Restriction enzyme accessibility assay was used to examine the impacts of Rhp26 CS mutations on its chromatin remodelling activity. Chromatin remodellers, such as Rhp26, can displace histones and allow for restriction sites to be exposed and cleaved by restriction enzymes, resulting in short DNA fragments (i.e. disappearance of upper bands and increased intensity of lower bands). The percentage of HaeIII digestion would be a great

measurement for active chromatin remodellers. As shown in Figure 1.5, we observed a significant loss in chromatin remodelling activity in all Rhp26 CS mutants tested (Figure 1.5A). Statistical significance in chromatin remodelling activity is observed across all Rhp26 CS mutants ($P<0.01$) when compared to Rhp26$^{\Delta 1\text{-}16}$ (Figure 1.5B). Out of the six mutations, A713P is the least detrimental, preserving about 60% of remodelling activity relative to the positive control Rhp26$^{\Delta 1\text{-}16}$. It also has the highest remodelling activity across all six Rhp26 CS mutants.

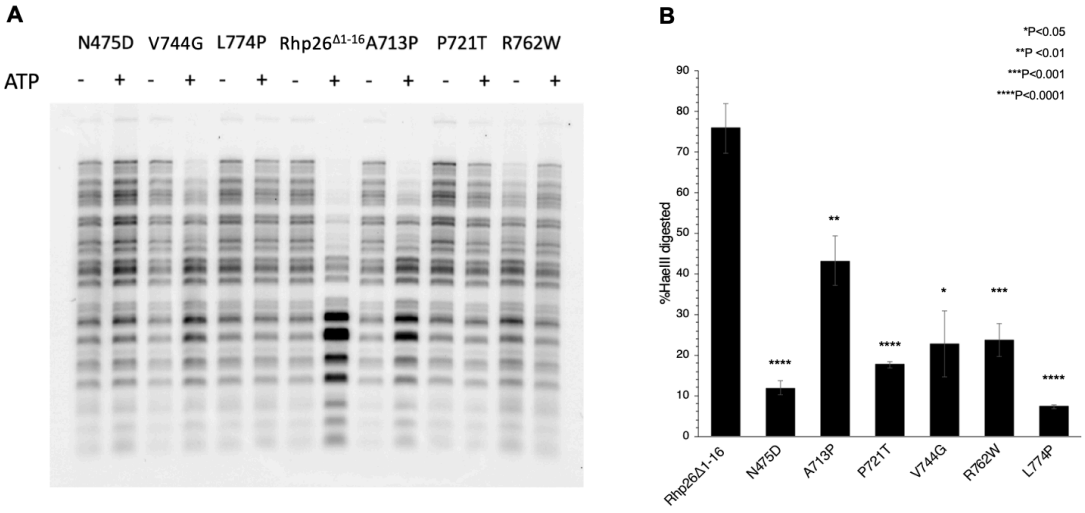

Figure 1.5. Chromatin remodelling activity in Rhp26 CS mutants as assessed by REAA. (A) Native gel showing the chromatin remodelling activity of Rhp26$^{\Delta 1}$-16 and CS mutants with and without ATP. (B) Quantitative evaluation of HaeIII digestion using three independent repeats. Statistical significance with Rhp26$^{\Delta 1\text{-}16}$ is indicated by asterisk(s).

DNA translocase activity was measured by Triplex Disruption Assay. Displacement of TFO as Rhp26 translocates across the triple helix is indicative of translocase activity. Rhp26 translocates across DNA in an ATP-dependent manner. Significant loss of DNA translocase activity in Rhp26 CS mutants is evidenced by the lowered intensity of the free TFO band (Figure 1.6A). Statistical significance in translocase activity is observed across all Rhp26 CS mutants ($P<0.01$) compared to Rhp26$^{\Delta 1\text{-}16}$ (Figure 1.6B). Out of the six mutations, A713P is the least detrimental, preserving about 50% of translocase activity relative to Rhp26$^{\Delta 1\text{-}16}$. It

also has the highest translocase activity across all six Rhp26 CS mutants. Note that multiple minor top bands indicate a small portion of DNA duplex was annealed with more than one TFO. Interestingly, these higher bands can be also displaced by Rhp26$^{\Delta 1\text{-}16}$ in an ATP-dependent manner.

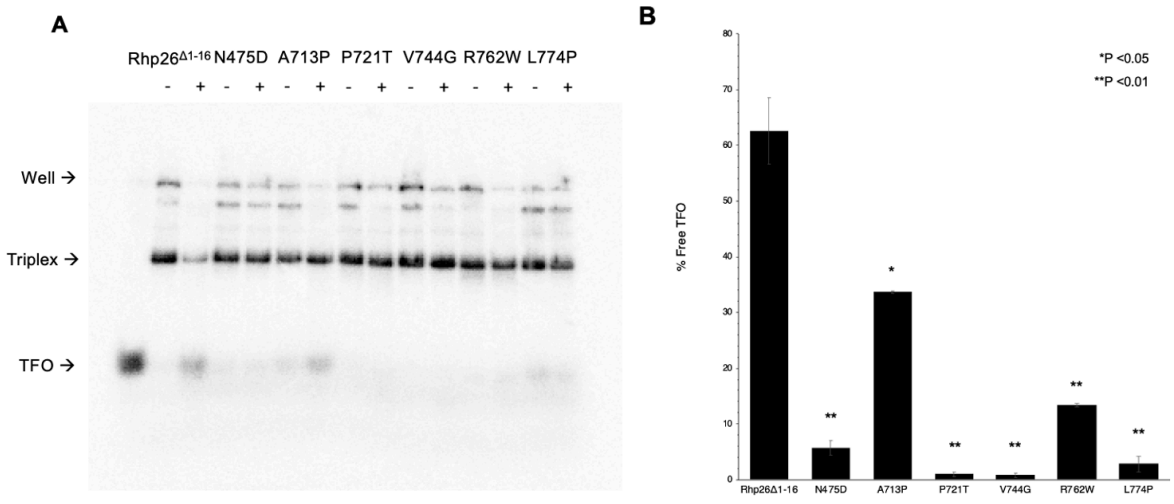

Figure 1.6. DNA translocase activity in Rhp26 CS mutants as assessed by Triplex Disruption Assay. (A) Native gel showing the DNA translocation activity of Rhp26$^{\Delta 1\text{-}}$16 and CS mutants with and without ATP. (B) Quantitative evaluation of TFO displacement using three independent repeats. Statistical significance with Rhp26$^{\Delta 1\text{-}16}$ is indicated by asterisk(s).

1.4 Discussion

We showed that both N475D and L774P exhibit decreased DNA binding affinities compared to Rhp26$^{\Delta 1\text{-}16}$. The location of these Rhp26 CS mutants might also give interesting insights on how DNA binding affinity is weakened. Asn475 is located in the helicase III motif of Rhp26, and is in close proximity with the sugar phosphate backbone of the template strand (Figure 1.3B). The change from polar, uncharged asparagine to negatively charged aspartic acid could negatively impact its interaction with DNA. Leu774 is located on an alpha helix downstream of the helicase VI motif. The change from leucine to proline on an alpha helix could potentially change the helix structure and affect the conformation of the DNA binding site of Rhp26.

We further demonstrate that all six mutations have decreased chromatin remodelling and DNA translocase activities. Because both activities require ATP, mutations to the core ATPase region are expected to be detrimental to activities that require its function. This is also consistent with previous results demonstrating a decreased ATPase activity in V744G (Lake et al., 2010). Interestingly, we observed a wide spectrum of activity reduction among these mutants.

N475D and L774P have weakened DNA binding affinities, and are therefore unable to interact with DNA to execute DNA translocation and chromatin remodelling events. Although not tested, the DNA binding affinities of other CS mutants are also expected to be impaired and impact chromatin remodelling and DNA translocase activities. Arg762 is located within an alpha helix that is positioned next to the non-template strand in the transcription bubble, and the change from a positively charged arginine to an amphipathic tryptophan can disrupt the hydrogen bond that stabilized DNA-Rhp26 interactions. Pro721 is located in the linker connecting a beta sheet and an alpha helix in close proximity with the transcription scaffold, and the mutation from proline to threonine can affect the conformation of the linker turn. Val744 is located at the end of a beta sheet. The mutation from valine to glycine may affect the stacking of the beta sheet and its subsequent conformation. Both P721T and V774G mutations alter local secondary structures that impact how Rhp26 interacts with DNA.

Interestingly, A713P has the least effect on the chromatin remodelling and DNA translocase activity of Rhp26 out of all the CS mutants (Figures 1.5B and 1.6B). Ala713 is located in the linker region between two alpha helices that directly interact with the transcription scaffold. Since the linker is flexible, an alanine to proline mutation should not have much interference with the folding and overall structure of Rhp26, therefore producing a Rhp26 CS mutant with the least biochemistry defect. However, the patient harboring this CSB mutation is compound heterozygous for CSB (with p.Phe665_Gln723del) and has the

most severe subtype of CS. It is likely that the deletion contributes to the significant defect in CSB function and causes the severe clinical phenotype. While studying these Rhp26 mutations *in vitro* can give a clearer insight into how the mutant proteins function biochemically, CS is an autosomal recessive disease, and clinical phenotypes are often a combination of the result of both mutant alleles. While there are some CS patients who are homozygous for CSB mutations, there are still a significant number of CS patients who are compound heterozygous for CSB. It is difficult to assess how the two different mutations may have interacted together to produce the observed clinical phenotype, or to specifically attribute particular symptoms to one of the mutations. Since only point mutations are generated in this study, a more comprehensive library of CSB mutations should be generated to test the biochemistry of these mutants, so that the relationship between patient genotypes and clinical phenotypes can be better understood. Another future direction for this project would be to use alanine scanning to assess the importance of single mutated residues on the overall structure and function of Rhp26.

CHAPTER 2: Regulation of Rad26/Pol II Interactions by Rad26Flanking Regions

2.1 Introduction

TC-NER is a transcription-dependent DNA repair mechanism that repairs bulky, helix distorting DNA damages. The mammalian model for TC-NER proposes CSB as a candidate for the initial recognition of the arrested Pol II (Hanawalt and Spivak, 2008). It suggests that CSB assists in TC-NER by modifying local chromatin structure to facilitate the repair process. Rad26 is the *Saccharomyces cerevisiae* ortholog of human CSB. It consists of 1085 amino acids with a core ATPase domain consisting of seven distinct helicase motifs shared by members of its SNF2 parent family (Andersen, 2017; Vangool et al., 1994). The leucine latch motif, first identified in the N terminus of Rhp26, the *S. pombe* homolog of CSB, is a key regulatory component of CSB (Wang et al., 2014). The leucine latch is shown to auto-inhibit ATPase and chromatin remodeling activities of Rhp26, and mutations to the leucine latch restored chromatin remodeling activity in Rhp26 (Wang et al., 2014). A CSB family specific coupling motif at the C-terminal region (CTR), involving residues 900-910 in Rhp26, was also identified to be essential for chromatin remodeling activity (Wang et al., 2019). Because these activities are essential for Rad26 to work in tandem with Pol II to resolve transcriptional arrests, we wondered if the CTR flanking regions of Rad26 can regulate Rad26/Pol II interactions. Additionally, previous work in our lab has solved the partial Cryo-EM structure of Rad26/Pol II, but the flanking regions were highly mobile and not visualized in the Cryo-EM structure (Xu et al., 2017). To examine the role of flanking regions in regulating Rad26/Pol II interactions, we measured the binding affinity between CTR truncations of Rad26 and Pol II elongation complex. It is found that residues 911-1085 in Rad26 are not critical for Rad26/Pol II complex formation. In contrast, the CTR coupling motif is important, but not essential, in promoting Rad26/Pol II interactions.

2.2 Materials and Methods

Protein expression and purification

Rad26 truncations were generated by PCR with primers in table 2.1. The template, full length Rad26, was cloned into pGEX-6P1 followed by a PreScission Protease recognition sequence and a N-terminus His-GST tag. PCR generated Rad26 truncations were confirmed with sequencing. Recombinant Rad26 proteins were transformed into Rosetta 2 DE3 competent cells (Novagen) for expression. Cells were grown in LB at 37°C until OD_{600} reached 0.8 and protein expression was induced by 0.5 mM of IPTG at 25°C for 16 hours. Cells were lysed using a microfluidizer in lysis buffer (500 mM NaCl, 20 mM Tris-HCl (pH 7.5), 5% glycerol, 1 mM DTT). Lysate supernatant was applied to a Ni-NTA agarose column (Qiagen) and equilibrated in purification buffer (lysis buffer with 10 mM imidazole) at 4°C for 1 hour. The column was washed with 30 column volumes of purification buffer, followed by protein elution in elution buffer (lysis buffer with 250 mM imidazole) and overnight PreScission Protease digestion to remove N-terminal His-GST tag. Protein eluates were then equilibrated to 300 mM NaCl and loaded onto a HiTrap Heparin affinity column (GE Healthcare). Rad26 constructs were eluted in a 300 - 1000 mM linear NaCl lysis buffer gradient. Protein purity was confirmed with SDS-PAGE.

Table 2.1. Primer sequences used in generating Rad26 constructs.

Rad26 Truncation	Forward Primer (5' to 3')	Reverse Primer (5' to 3')
$Rad26^{1-899}$	GGAGGAGAGAGCAATTTATA AACCGTTATGAGTCATG	ATAAATTGCTCTCTCCTCCTAG CAACCCTTCG
$Rad26^{1-910}$	GTCATGATTCGGTTGTCAATT AGCACGCGGGCAGTTCTTC	CTAATTGACAACCGAATCATGA CTCATAACGGTTTCTAAATTGC

Electrophoretic Mobility Shift Assay (EMSA)

Transcriptional scaffold was formed by annealing radioactively labelled RNA with template and non-template DNA at 95°C for 5 minutes, then slowly cooling down to room temperature. Pol II elongation complex was constructed by incubating radiolabeled transcriptional scaffold to 10 subunit Pol II in a 2:3 molar ratio at room temperature for 10 minutes in binding buffer (20mM Tris-HCl (pH 7.5), 5mM MgCl2, 5mM DTT, 40mM KCl, 50mM NaCl, 5% glycerol, 0.1 mg/ml BSA). 10 nM Pol II elongation complex was incubated with various concentrations of Rad26 (5, 10, 15, 25, 50, 100 nM). Reactions were carried out at room temperature for 30 minutes, resolved on a 4.5% native PAGE gel in 0.5X TBE buffer (pH 8.0) at 4°C for 2 hours, and visualized using a phosphor screen and PharosFX imager. Results were quantified using Bio-Rad ImageLab. Statistical significance was calculated using a two-tailed T-test.

2.3 Results

By examining the formation of Rad26/Pol II complexes, we can observe the effects of Rad26 flanking regions on the interaction between Rad26 and Pol II. Two Rad26 CTR truncations, $Rad26^{1-899}$ and $Rad26^{1-910}$ were tested. Sequence alignment shows that the coupling motif, with the conserved H/D residues, is located in similar residue numbers in both Rad26 and Rhp26 (Figure 2.1B). The two truncations generated, $Rad26^{1-899}$ and $Rad26^{1-910}$, test the effect of the coupling motif and the rest of the CTR (911-1085) on the interaction between Rad26 and Pol II.

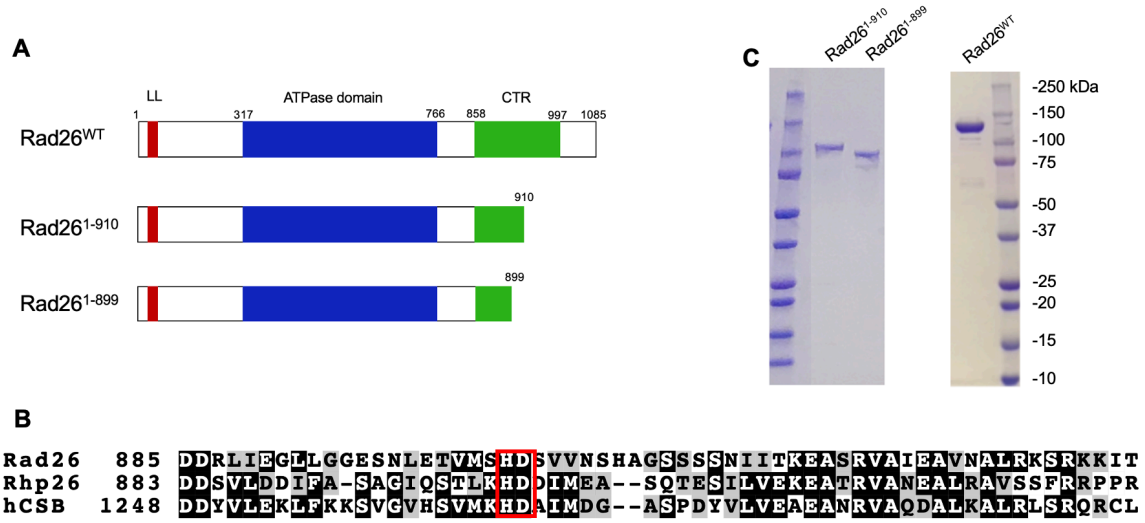

Figure 2.1. Wild-type Rad26 and truncations generated in this study. (A) Schematic of Rad26^{WT}, Rad26$^{1-899}$and Rad26$^{1-910}$. The leucine latch motif, core ATPase domain with the seven conserved helicase motifs and C-terminal region shown in red, blue and green respectively. (B) Sequence alignment of Rad26 (*S. cerevisiae*), Rhp26 (*S. pombe*) and human CSB showing the conserved H/D residues in the coupling motif boxed in red. (C) SDS-PAGE of purified Rad26^{WT}, Rad26$^{1-899}$, and Rad26$^{1-910}$. Like purified Rhp26 in Chapter 2, Rad26 also suffers from a small degree of degradation *in vitro*.

At low Rad26 concentrations (5, 10, and 15 nM), no Rad26/Pol II complexes are formed (Figure 2.2A). Rad26/Pol II complex formation starts at the addition of 25 nM of Rad26 in Rad26$^{1-910}$, but not in Rad26^{WT} and Rad26$^{1-899}$, where Rad/26 Pol II complex formation starts at 50 nM of Rad26.

At 50 nM of Rad26 added, there is a statistically significant difference in % of Rad26/Pol II complex formation between Rad26$^{1-899}$ and both Rad26^{WT} and Rad26$^{1-910}$ (Figure 2.2B), but no statistical significance is observed between Rad26^{WT} and Rad26$^{1-910}$. The same is observed when Rad26 concentration increases to 100 nM. Smearing is observed in the resolution of Rad26^{WT}/Pol II complexes at higher Rad26^{WT} concentrations (50 and 100 nM), but not in truncated Rad26/Pol II complexes.

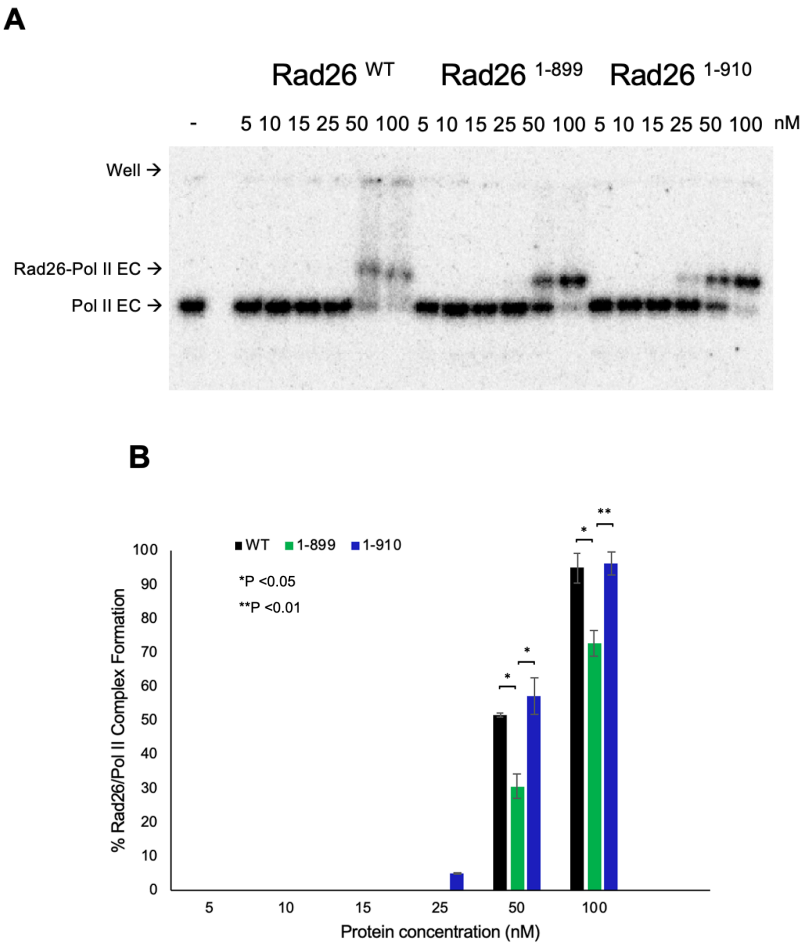

Figure 2.2. Interactions between wild-type Rad26 and truncations with Pol II. (A) Native gel showing the formation of Rad26/Pol II complexes in varying Rad26 concentrations. (B) Quantitative evaluation of Rad26/Pol II complex formation using three independent repeats. Statistical significance is indicated by asterisk(s).

2.4 Discussion

From the electrophoretic mobility shift assay, Rad26/Pol II interactions can be ranked in the following order: $Rad26^{1-910} \sim Rad26^{WT} > Rad26^{1-899}$. Regardless of Rad26 variety, critical concentration of Rad26 needs to be reached before complex formation can occur (Figure 2.2A).

$Rad26^{WT}$ and $Rad26^{1-910}$ have similar binding affinities to Pol II, as indicated by the lack of statistical significance and the similar % of Rad26/Pol II complex formation. Deletion of residues 911-1085 in the CTR did not negatively impact complex formation, indicating that it is likely not essential for Rad26 to interact with Pol II. Previous work suggests that the deletion of this homologous region in Rhp26 is not detrimental to its chromatin remodeling activity (Wang et al., 2019). Interestingly, $Rad26^{1-910}$ is able to start forming Rad26/Pol II complex at a lower concentration than $Rad26^{WT}$. It is possible that residues 911-1085 of the CTR could be inhibiting the interaction between Rad26 and Pol II at low Rad26 concentrations, and removal of this region eliminates the inhibitory effect it has on Rad26/Pol II interaction, although more studies would need to be done to examine this hypothesis.

On the other hand, $Rad26^{1-899}$ shows a decreased ability in forming Rad26/Pol II complexes compared to both $Rad26^{WT}$ and $Rad26^{1-910}$, and also requires a higher Rad26 concentration to start complex formation. The coupling motif, essential in chromatin remodeling activities, is also important in promoting Rad26/Pol II interaction. Deletion of the coupling motif in $Rad26^{1-899}$ could have impeded the interactions between $Rad26^{1-899}$ and Pol II, therefore requiring a higher starting concentration of $Rad26^{1-899}$ to form stable Rad26/Pol II complexes. Considering that $Rad26^{1-899}$ also lacks residues 911-1085, which removes the hypothesized inhibitory effect it has on Rad26/Pol II interactions, the importance of the coupling motif in promoting Rad26/Pol II interactions may be higher than what is shown in Figure 3.2.

High molecular weight oligomerization is seen when higher concentrations of $Rad26^{WT}$ (50 and 100 nM) are added (Figure 2.2A). It could indicate that residues 911-1085 of the Rad26 CTR serve some function in facilitating oligomerization of Rad26 with itself established $Rad26^{WT}$/Pol II complex, contributing to the high molecular weight oligomerization detected.

Unfortunately, I was only able to test two truncations of the CTR, which does not provide a full picture of the role of flanking regions on regulating Rad26/Pol II interactions. Since the coupling motif essential for Rad26 activity also has regulatory effects on Rad26/Pol II interactions, it is possible that the leucine latch, an inhibitor of chromatin remodeling, can regulate the same interactions. More Rad26 truncations should be tested to systematically identify more residues within the flanking regions that influence Rad26/Pol II interactions. Specifically, double truncations of deleting both the leucine latch and coupling motif should be tested to observe if there are compensatory or synergistic effects when both regulatory motifs are deleted. Coupling EMSA with other biochemical tests can also test the function of truncated Rad26s in addition to their interactions with Pol II.

Chapter 2 is co-authored with Xu, Jun. The thesis author was the primary author of this chapter.

REFERNECES

Andersen, K. R. 2017. Insights into Rad3 kinase recruitment from the crystal structure of the DNA damage checkpoint protein Rad26. *Journal of Biological Chemistry,* 292(20)**,** pp 8149-8157.

Calmels, N., Botta, E., Jia, N., Fawcett, H., Nardo, T., Nakazawa, Y., Lanzafame, M., Moriwaki, S., Sugita, K., Kubota, M., Obringer, C., Spitz, M. A., Stefanini, M., Laugel, V., Orioli, D., Ogi, T. & Lehmann, A. R. 2018. Functional and clinical relevance of novel mutations in a large cohort of patients with Cockayne syndrome. *Journal of Medical Genetics,* 55(5)**,** pp 329-343.

Chatterjee, N. & Walker, G. C. 2017. Mechanisms of DNA Damage, Repair, and Mutagenesis. *Environmental and Molecular Mutagenesis,* 58(5)**,** pp 235-263.

Cleaver, J. E., Lam, E. T. & Revet, I. 2009. Disorders of nucleotide excision repair: the genetic and molecular basis of heterogeneity. *Nature Reviews Genetics,* 10(11)**,** pp 756-768.

de Waard, H., de Wit, J., Andressoo, J. O., van Oostrom, C. T. M., Riis, B., Weimann, A., Poulsen, H. E., van Steeg, H., Hoeijmakers, J. H. J. & van der Horst, G. T. J. 2004. Different effects of CSA and CSB deficiency on sensitivity to oxidative DNA damage. *Molecular and Cellular Biology,* 24(18)**,** pp 7941-7948.

Eisen, J. A., Sweder, K. S. & Hanawalt, P. C. 1995. EVOLUTION OF THE SNF2 FAMILY OF PROTEINS - SUBFAMILIES WITH DISTINCT SEQUENCES AND FUNCTIONS. *Nucleic Acids Research,* 23(14)**,** pp 2715-2723.

Gorbalenya, A. E. & Koonin, E. V. 1993. HELICASES - AMINO-ACID-SEQUENCE COMPARISONS AND STRUCTURE-FUNCTION-RELATIONSHIPS. *Current Opinion in Structural Biology,* 3(3)**,** pp 419-429.

Hanawalt, P. C. & Spivak, G. 2008. Transcription-coupled DNA repair: two decades of progress and surprises. *Nature Reviews Molecular Cell Biology,* 9(12)**,** pp 958-970.

Hauk, G. & Bowman, G. D. 2011. Structural insights into regulation and action of SWI2/SNF2 ATPases. *Current Opinion in Structural Biology,* 21(6)**,** pp 719-727.

He, C. X., Sun, M., Wang, G. X., Yang, Y., Yao, L. B. & Wu, Y. M. 2017. Two novel mutations in ERCC6 cause Cockayne syndrome B in a Chinese family. *Molecular Medicine Reports,* 15(6)**,** pp 3957-3962.

Horibata, K., Iwamoto, Y., Kuraoka, I., Jaspers, N. G. J., Kurimasa, A., Oshimura, M., Ichihashi, M. & Tanaka, K. 2004. Complete absence of Cockayne syndrome group B gene product gives rise to UV-sensitive syndrome but not Cockayne syndrome. *Proceedings of the National Academy of Sciences of the United States of America,* 101(43)**,** pp 15410-15415.

Karikkineth, A. C., Scheibye-Knudsen, M., Fivenson, E., Croteau, D. L. & Bohr, V. A. 2017. Cockayne syndrome: Clinical features, model systems and pathways. *Ageing Research Reviews,* 33(3-17.

Kusakabe, M., Onishi, Y., Tada, H., Kurihara, F., Kusao, K., Furukawa, M., Iwai, S., Yokoi, M., Sakai, W. & Sugasawa, K. 2019. Mechanism and regulation of DNA damage recognition in nucleotide excision repair. *Genes and Environment,* 41(

Lake, R. J. & Fan, H. Y. 2013. Structure, function and regulation of CSB: A multi-talented gymnast. *Mechanisms of Ageing and Development,* 134(5-6)**,** pp 202-211.

Lake, R. J., Geyko, A., Hemashettar, G., Zhao, Y. & Fan, H. Y. 2010. UV-Induced Association of the CSB Remodeling Protein with Chromatin Requires ATP-Dependent Relief of N-Terminal Autorepression. *Molecular Cell,* 37(2)**,** pp 235-246.

Laugel, V. 2013. Cockayne syndrome: The expanding clinical and mutational spectrum. *Mechanisms of Ageing and Development,* 134(5-6)**,** pp 161-170.

Laugel, V., Dalloz, C., Durand, M., Sauvanaud, F., Kristensen, U., Vincent, M. C., Pasquier, L., Odent, S., Cormier-Daire, V., Gener, B., Tobias, E. S., Tolmie, J. L., Martin-Coignard, D., Drouin-Garraud, V., Heron, D., Journel, H., Raffo, E., Vigneron, J., Lyonnet, S., Murday, V., Gubser-Mercati, D., Funalot, B., Brueton, L., del Pozo, J. S., Munoz, E., Gennery, A. R., Salih, M., Noruzinia, M., Prescott, K., Ramos, L., Stark, Z., Fieggen, K., Chabrol, B., Sarda, P., Edery, P., Bloch-Zupan, A., Fawcett, H., Pham, D., Egly, J. M., Lehmann, A. R., Sarasin, A. & Dollfus, H. 2010. Mutation Update for the CSB/ERCC6 and CSA/ERCC8 Genes Involved in Cockayne Syndrome. *Human Mutation,* 31(2)**,** pp 113-126.

Leadon, S. A. & Lawrence, D. A. 1992. STRAND-SELECTIVE REPAIR OF DNA DAMAGE IN THE YEAST GAL7-GENE REQUIRES RNA POLYMERASE-II. *Journal of Biological Chemistry,* 267(32)**,** pp 23175-23182.

Licht, C. L., Stevnsner, T. & Bohr, V. A. 2003. Cockayne syndrome group B cellular and biochemical functions. *American Journal of Human Genetics,* 73(6)**,** pp 1217-1239.

Ma, H. X., Hu, Z. B., Wang, H. F., Jin, G. F., Wang, Y., Sun, W. W., Chen, D., Tian, T., Jin, L., Wei, Q. Y., Lu, D. R., Huang, W. & Shen, H. B. 2009. ERCC6/CSB gene polymorphisms and lung cancer risk. *Cancer Letters,* 273(1)**,** pp 172-176.

Marteijn, J. A., Lans, H., Vermeulen, W. & Hoeijmakers, J. H. J. 2014. Understanding nucleotide excision repair and its roles in cancer and ageing. *Nature Reviews Molecular Cell Biology,* 15(7)**,** pp 465-481.

Nance, M. A. & Berry, S. A. 1992. COCKAYNE SYNDROME - REVIEW OF 140 CASES. *American Journal of Medical Genetics,* 42(1)**,** pp 68-84.

Newman, J. C., Bailey, A. D. & Weiner, A. M. 2006. Cockayne syndrome group B protein (CSB) plays a general role in chromatin maintenance and remodeling. *Proceedings of the National Academy of Sciences of the United States of America,* 103(25)**,** pp 9613-9618.

Scheibye-Knudsen, M., Croteau, D. L. & Bohr, V. A. 2013. Mitochondrial deficiency in Cockayne syndrome. *Mechanisms of Ageing and Development,* 134(5-6)**,** pp 275-283.

Thoma, N. H., Czyzewski, B. K., Alexeev, A. A., Mazin, A. V., Kowalczykowski, S. C. & Pavletich, N. P. 2005. Structure of the SWI2/SNF2 chromatin-remodeling domain of eukaryotic Rad54. *Nature Structural & Molecular Biology,* 12(4)**,** pp 350-356.

van der Weegen, Y., Golan-Berman, H., Mevissen, T. E. T., Apelt, K., Gonzalez-Prieto, R., Goedhart, J., Heilbrun, E. E., Vertegaal, A. C. O., van den Heuvel, D., Walter, J. C., Adar, S. & Luijsterburg, M. S. 2020. The cooperative action of CSB, CSA, and UVSSA target TFIIH to DNA damage-stalled RNA polymerase II. *Nature communications,* 11(1)**,** pp 2104.

Vangool, A. J., Verhage, R., Swagemakers, S. M. A., Vandeputte, P., Brouwer, J., Troelstra, C., Bootsma, D. & Hoeijmakers, J. H. J. 1994. RAD26, THE FUNCTIONAL SACCHAROMYCES-CEREVISIAE HOMOLOG OF THE COCKAYNE-SYNDROME-B GENE ERCC6. *Embo Journal,* 13(22)**,** pp 5361-5369.

Wang, L. F., Limbo, O., Fei, J., Chen, L., Kim, B., Luo, J., Chong, J., Conaway, R. C., Conaway, J. W., Ranish, J. A., Kadonaga, J. T., Russell, P. & Wang, D. 2014. Regulation of the Rhp26(ERCC6/CSB) chromatin remodeler by a novel conserved leucine latch motif. *Proceedings of the National Academy of Sciences of the United States of America,* 111(52)**,** pp 18566-18571.

Wang, W., Xu, J., Limbo, O., Fei, J., Kassavetis, G. A., Chong, J., Kadonaga, J. T., Russell, P., Li, B. & Wang, D. 2019. Molecular basis of chromatin remodeling by Rhp26, a yeast CSB ortholog. *Proceedings of the National Academy of Sciences of the United States of America,* 116(13)**,** pp 6120-6129.

Waterhouse, A., Bertoni, M., Bienert, S., Studer, G., Tauriello, G., Gumienny, R., Heer, F. T., de Beer, T. A. P., Rempfer, C., Bordoli, L., Lepore, R. & Schwede, T. 2018. SWISS-MODEL: homology modelling of protein structures and complexes. *Nucleic Acids Research,* 46(W1)**,** pp W296-W303.

Weidenheim, K. M., Dickson, D. W. & Rapin, I. 2009. Neuropathology of Cockayne syndrome: Evidence for impaired development, premature aging, and neurodegeneration. *Mechanisms of Ageing and Development,* 130(9)**,** pp 619-636.

Wilson, B. T., Lochan, A., Stark, Z. & Sutton, R. E. 2016a. Novel Missense Mutations in a Conserved Loop Between ERCC6 (CSB) Helicase Motifs V and VI: Insights Into Cockayne Syndrome. *American Journal of Medical Genetics Part A,* 170(3)**,** pp 773-776.

Wilson, B. T., Stark, Z., Sutton, R. E., Danda, S., Ekbote, A. V., Elsayed, S. M., Gibson, L., Goodship, J. A., Jackson, A. P., Keng, W. T., King, M. D., McCann, E., Motojima, T., Murray, J. E., Omata, T., Pilz, D., Pope, K., Sugita, K., White, S. M. & Wilson, I. J. 2016b. The Cockayne Syndrome Natural History (CoSyNH) study: clinical findings in 102 individuals and recommendations for care. *Genetics in Medicine,* 18(5)**,** pp 483-493.

Xu, J., Lahiri, I., Wang, W., Wier, A., Cianfrocco, M. A., Chong, J., Hare, A. A., Dervan, P. B., DiMaio, F., Leschziner, A. E. & Wang, D. 2017. Structural basis for the initiation of eukaryotic transcription-coupled DNA repair. *Nature,* 551(7682)**,** pp 653-+.